Journal of Mining Science, Vol. 35, No. 2, 1999

MODELING OF INITIAL STRESSES AND WEAKENING SURFACES BY FINITE-ELEMENT METHOD

I. L. Boltengagen

UDC 622.831

Solutions of geomechanical problems in terms of full and additional displacements are compared for the example of the creation of the mined-out space filled with stowing and the construction of a subway tunnel. An approach to modeling the contact interaction of a block massif is proposed. Data on the stress-strain state of rock mass in forming the mined-out spaces close to extended geological disturbances are presented.

INTRODUCTION

Preliminary Stress State of Rock Mass

The preliminary stress state of rock mass is the main feature of geomechanical problems. The initial stress, strain, and displacement fields created in the rock mass during the geological development of the lithosphere change by a quantity of additional stresses, strains and displacements during the technogenic action on the rock mass. In numerical modeling to investigate the geomechanical state of the rock mass, the "direct" formulation of the problem and the formulation in terms of the additional stresses must be distinguished [1]. In the direct formulation, the calculation region with subregions characterized by different deformational properties is loaded by surface forces at the boundary and mass forces distributed over the volume after the mined-out spaces are created in the calculation region. It is more correct to formulate the problem in terms of additional stresses, taking account of the initial stress state of rock mass before the formation of the cavities in it, when all the changes are regarded as the result of loading the calculation region over the surfaces of the newly formed workings. In some cases, the difference in the results obtained in the two formulations is negligible. The technology for creation of cavities filled with artificial materials in the rock mass must also be taken into account in analyzing the geomechanical situation. In the present work, the differences in the solutions of the geomechanical problems obtained in the direct formulation and in terms of additional stresses, taking account of the cavity formation technology, are considered, for the example of modeling the mined-out space filled with stowing and the construction of a subway tunnel.

Geological Disturbances in Rock Mass

Such disturbances are significant in geomechanical problems. The contact-elements traditionally used in the finite-element method (FEM) require the introduction of the deformational and strength properties of the contact in the calculation scheme; these properties are characterized by the dependences of the relative normal displacement of the fracture sides on the normal component of the surface force vector and the relative tangential shift of the fracture sides on the tangential component of the surface force vector, at various normal pressures [2]. Practical difficulties are entailed with determining the corresponding data on the properties of the geological disturbance in-situ. Passing in the limit to a geological disturbance of zero thickness, the contact properties reduce to three possibilities of behavior with variation in the initial stress state of the rock mass in cavity creation: 1) stiff cohesion of the fracture sides (ensuring continuity of the additional displacement vector in the rock mass at contact); 2) opening of the fracture (zero surface force vector in the rock mass at contact); 3) shift of the fracture sides (the tangential and normal components of the surface force vector are related by the Coulomb shear strength criterion, and the normal component of the displacement vector is continuous at the contact). In the article, data on the stress-strain state (SSS) of rock mass are given for the example of mined-out spaces close to extended geological disturbances with the use of proposed approximate approach to modeling of the contact interaction of the block mass.

Institute of Mining, Siberian Branch, Russian Academy of Sciences, Novosibirsk. Translated from Fiziko-Tekhnicheskie Problemy Razrabotki Poleznykh Iskopaemykh, No. 2, pp. 49-59, March-April, 1999. Original article submitted June 30, 1998.

1062-7391/99/3502-0150$22.00

1. INFLUENCE OF THE CAVITY CREATION TECHNOLOGY ON THE SSS OF THE FILLING ARTIFICIAL MATERIALS

In the direct formulation of geomechanical problems, the initial SSS of the rock mass is taken into account by the corresponding conditions at the external boundaries of the region of solution, which are a considerable distance from the investigated section of rock mass. In the solution in terms of the additional stresses, FEM allows the initial rock mass SSS to be taken into consideration by introducing an elementary component due to the initial stresses or initial strains within the element in the nodal forces [3]

$$\int B^T \sigma_{ij}^0 dV \quad \text{and} \quad \int B^T D\varepsilon_{ij}^0 dV.$$

In a self-balanced initial stress system, the total contribution of the elements containing the given node due to the initial stresses and gravitational forces is zero. The force balance is disrupted at the boundaries of the cavities formed in the solution region by removing material.

Mined-out Space Filled with Solidifying Stowing

Such mined-out spaces are constituent part of the reserve extraction technology used at ore deposits. The influence of the sequence in which the artificial massif is created on its SSS was investigated in [4]. The computations required to take account of the technology for filling the mined-out space with solidifying stowing are considerably more extensive than in the direct formulation, and the difference in the results is sometimes negligible. The goal here is to establish the applicability of the direct formulation of the solution to the analysis of the geomechanical conditions at the Talnakh deposits. The following calculation scheme was used. A mined-out space of thickness 25 m is sequentially filled with stowing as its horizontal ledge extent increases from 50–100 to 500 m. The elastic modulus E_m Poisson's ratio ν_m, and specific weight γ_m of the rock mass are 40 GPa, 0.25, and 0.027 MPa/m, respectively. The difference in the solutions in the following formulations of the problem was analyzed:

1) Direct formulation of the problem (the calculation region is loaded by gravitational forces after creating the mined-out space filled with stowing);

2) The formulation in terms of additional stresses at the eventual moment of mining operation development (the calculation region is loaded by gravitational forces distributed in the rock mass and the initial stresses; in the mined-out space filled with stowing, the initial stresses are zero);

3) The formulation taking account of the sequence in which the artificial massif is created.

The latter case, based on the sequential cycle method [4], requires some explanations. The initial stress state of the rock mass σ_{ij}^0 changes by $\Delta\sigma_{ij}^0$ after the formation of the first cavity, and the stress state of the rock mass before the mined-out space is filled with stowing is determined by the relation $\sigma_{ij}^1 = \sigma_{ij}^0 + \Delta\sigma_{ij}^0$. After the mined-out space is expanded (the second cavity is created), the artificial mass that fills the first cavity is loaded by gravitational forces and the initial stresses σ_{ij}^1 distributed in the rock mass. As a result, the stresses change by $\Delta\sigma_{ij}^1$, and in the rock mass $\sigma_{ij}^2 = \sigma_{ij}^0 + \Delta\sigma_{ij}^0 + \Delta\sigma_{ij}^1$, the stresses in the stowing within the first chamber are $\Delta\sigma_{ij}^1$. After the third cavity is formed, the further additional loading of the filling mass in the first cavity the first additional load of the filling mass and in the second cavity occur. As a result of the creation of n cavities, the stress state of the rock mass is $\sigma_{ij}^n = \sigma_{ij}^0 + \Delta\sigma_{ij}^0 + \Delta\sigma_{ij}^1 + \ldots + \Delta\sigma_{ij}^{n-1}$; the stress on the stowing in the first cavity is $\sigma_{ij}^f = \Delta\sigma_{ij}^1 + \Delta\sigma_{ij}^2 + \ldots + \Delta\sigma_{ij}^{n-1}$; the stress on the stowing in the second cavity is $\sigma_{ij}^f = \Delta\sigma_{ij}^2 + \ldots + \Delta\sigma_{ij}^{n-1}$; the stress on the stowing in the $(n-1)$th cavity is $\sigma_{ij}^f = \Delta\sigma_{ij}^{n-1}$; the stowing in the nth cavity is not additionally loaded.

In consequence of the symmetry of the problem (symmetric development of the extraction fronts from the central line of the cut), we may consider half of the complete region of solution. For the first formulation, we use the following boundary conditions: 1) the upper horizontal boundary is stress-free: $\sigma_y = 0$, $\tau_{xy} = 0$; 2) at the left vertical boundary (the symmetry axis) and the right vertical boundary (2 km from the symmetry axis), $\tau_{xy} = 0$, $U = 0$; 3) at the lower horizontal boundary (at a depth of 4 km), the horizontal and vertical components of the displacement vector are $U = 0$ and $V = 0$. This ensured a hydrostatic stress state of the rock mass at depth Y

$$\sigma_x = \frac{\nu_m}{1-\nu_m}\gamma_m Y, \quad \sigma_y = \gamma_m Y. \tag{1}$$

To formulate the problem in terms of the additional stresses, the boundary conditions are analogous in the given initial stress state, except that the corresponding components of the additional stresses and displacements are

zero. The elements modeling the material removed (the creation of the working) are disregarded in forming the system of linear algebraic equations for calculating the nodal displacements; in the elements modeling the initial filling of the mined-out space with stowing, zero initial stresses were assumed. The contribution of the gravitational forces to the equilibrium equations was made in the traditional manner. The total number of nodes is 615; the number of triangular elements is 1163; and the minimum size of an element in the vicinity of the ledge is around 6 m.

The parameters of the basic calculation are as follows: the mined-out space is at a depth $H = 1$ km; reserve extraction and subsequent filling the mined-out space with stowing is carried out by chambers of width 50 m; the deformational properties of the stowing are: $E_f = 1$ GPa, $\nu_f = 0.2$, and specific weight is $\gamma_f = 0.02$ MPa/m. In Fig. 1*a*, the distributions of the vertical components of the stress tensor in the central horizontal cross-section of filling mass with a filled mined-out space of width 400 m are shown for each of the three formulations. The reaction of the filling mass for the third formulation is shown in Fig. 1*a* for an aperture greater in width than two extracted unites (100 m in the present case). In Fig. 1*b*, the corresponding results are shown for the case when the ledge mining is carried out with chambers of width 25 m. The difference in the stress state of artificial mass with the use of stowing with the higher strain modulus $E_f = 10$ GPa and with a small depth $H = 100$ m of the mined-out space in comparison with the extent is illustrated in Fig. 1*c*, *d*. For the latter case, we use a grid with fewer nodes and elements (571 and 1088, respectively), but with the same minimal size of the element close to the mined-out space.

Analysis of the results indicates that the difference in the solutions is slight on the first two formulations over a wide range of conditions. In the initial state, the vertical strain ε_m in the rock mass at a depth H is $\gamma_m H / E_m$. The difference in pressures in the stowing when using the first two formulations is determined by the ratio of the strain moduli of the surrounding and artificial masses: $\Delta P \approx E_f \cdot \varepsilon_m \approx \gamma_m H \cdot E_f / E_m$. The stowing used at the Norilsk mines with its grade strength after six months of hardening has strain modulus $E_f = 0.1$–1.0 GPa. When $E_f / E_m \approx 10^{-2}$, the difference in ΔP for depths up to 1.5 km is no more than 0.5 MPa; this corresponds to the difference in vertical stresses in the roof and floor of the filling mass due to its weight.

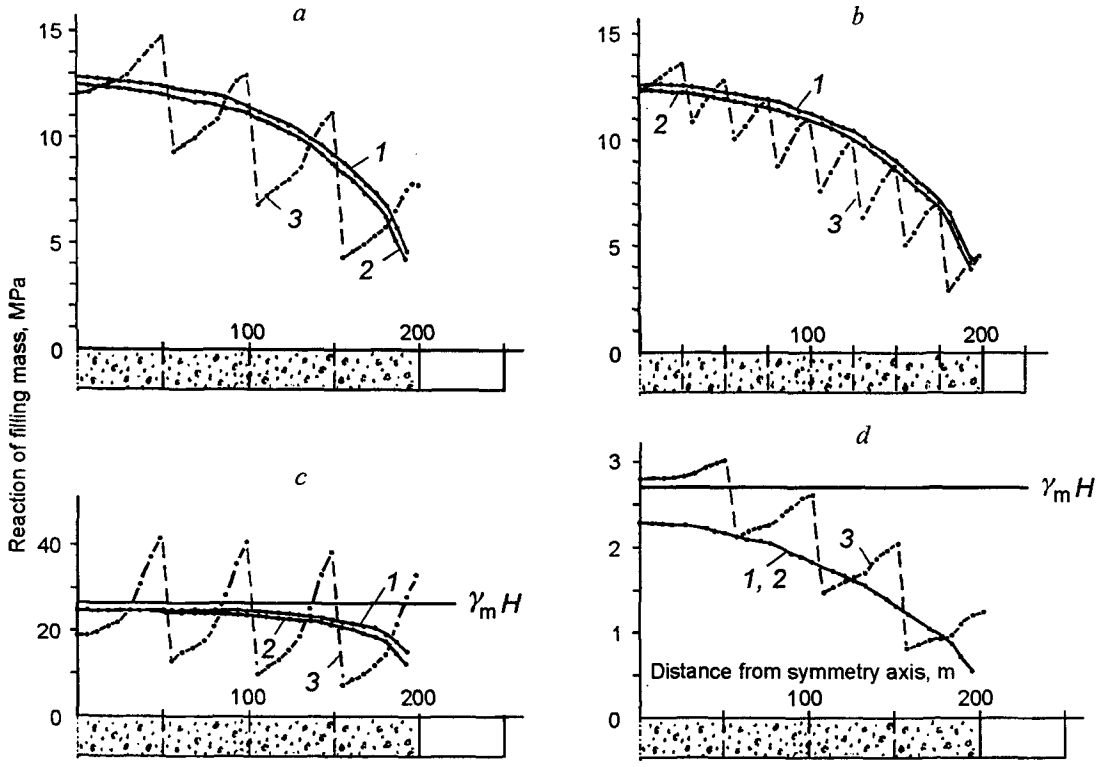

Fig. 1. Reaction of filling mass with successive increase in width of the mined-out space filled with stowing to 400 m, according to calculations in the direct formulation (*1*) and in terms of the final additional stress (*2*) and calculations where the sequence in which the artificial mass is created is taken into account (*3*).

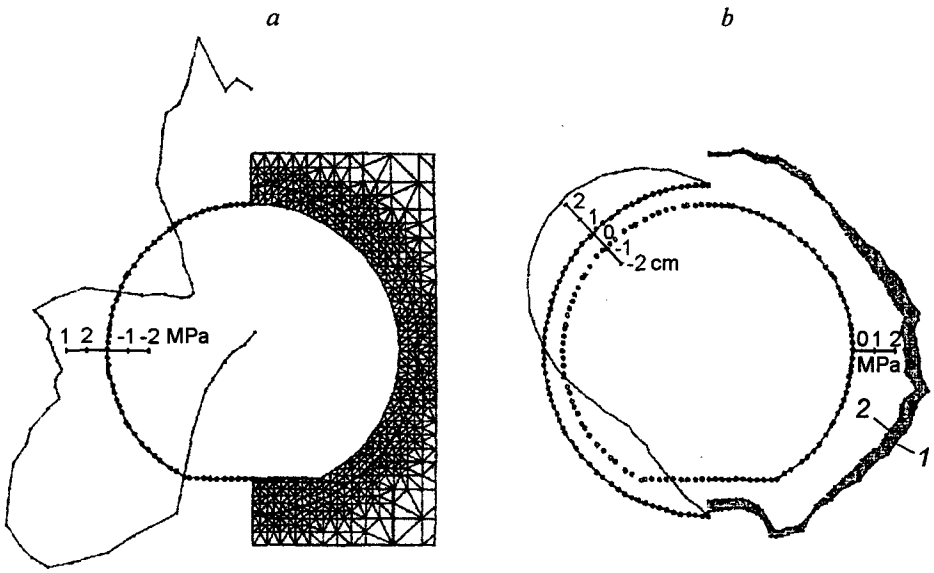

Fig. 2. Discretization of the region into triangular elements close to the tunnel (*a*, on the right), stress distribution at the inner tunnel contour in the direct formulation (*a*, on the left) and in terms of the additional stresses (*b*, on the right), disregarding (solid curve *1*) and taking account of (dash-dot curve *2*) slippage at the contact of soil massif with tunnel lining, and the distribution of soil massif shear at the contact (*b*, on the left).

The third formulation corresponds more accurately to the actual process of artificial mass formation but takes no account of factors such as the creep of the stowing, the variation in its strain properties associated with the increase in its rigidity over time and additional load, the formation of the filling mass in layers from the bottom to the top, and the presence of a protective ceiling and technological underfilling. Taking these factors into account is possible, but may lead to an unjustified increase in the volume of calculations required; moreover, errors in the model parameters may lead to a final result of limited value. Even for a simplified version of the third formulation in modeling development of mining operations, the error unavoidably accumulates at each stage of pilot winning chamber creation. The use of simpler formulations seems preferable. The first two formulations permit estimation of the state of the artificial mass, at least to mining widths no greater than half the depth of the ledge and for the stowing materials actually used at the Norilsk mines. The overestimated values obtained on average for the stresses in the stowing may be used to determine the state of the workings in the artificial mass. In the case where the depth is small relative to the width of the working or the strain moduli of the surrounding and artificial masses are of the same order, the sequence of filling mass formation must be taken into account in order to analyze its SSS. The difference in the solutions is even more significant when the strain modulus of the filling material considerably exceeds that of the surrounding rock mass.

Creation of Monolithic Concrete Tunnel Support by the Shield Method

This approach is economically favorable variant of subway construction in soil mass. The following geomechanical problem is solved: at a depth of 20 m, an annular monolithic concrete lining with external and internal radii of 2.95 and 2.6 m, respectively, is created. The distance from the center of the tunnel to the floor is 2.3 m. The total solution region is a rectangle (width 60 m, height 40 m). In Fig. 2*a* (at the right), the finite element grid in the vicinity of the tunnel is shown. On account of the symmetry, half of the total solution region has been considered. The number of nodes and grid elements is 810 and 1499, respectively; the minimum size of the elements in a lining of thickness 35 cm is around 6 cm. The properties of the rock mass and the lining are, respectively: $E_m = 10$ MPa, $\nu_m = 0.2$, $\gamma_m = 0.018$ MPa/m and $E_0 = 30$ GPa, $\nu_0 = 0.2$, $\gamma_0 = 0.02$ MPa/m.

One method of estimating the state of the tunnel is as follows. In the laboratory, a plane model of equivalent materials is created, ensuring absolute adhesion of the lining material and soil. The model is placed in a centrifuge or on a moving belt to simulate the gravitational forces acting in the rock mass; horizontal displacements at the lateral vertical boundaries of the model and vertical displacements at the lower horizontal boundary are not permitted. With plane deformation, this model ensures a hydrostatic stress state of the soil massif. The

mathematical analog of this model is solution of the problem in the direct formulation. In Fig. 2*a* (at the left), the stress distribution at the inner lining contour is shown for the given formulation of the problem. Note the unusual "three-lobe" curve: compression in the roof; tension in the upper sectors of the lining bounded by rays from the center of the tunnel at angles of 25 and 55° to the horizontal; compression in the edge; and tension in the floor. At smaller (by a factor of 10) values of the lining strain modulus, a customary "two-lobe" curve of stress distribution at the inner tunnel contour is formed: tensions in the roof and the floor, and compressions in the edges [5]. The result obtained is a consequence of the direct formulation of the problem: in modeling, the considerably less rigid soil massif moves downward under the action of gravitational forces, taking with it the tunnel.

The solution of the problem in terms of the additional stresses more adequately reflects the actual interaction between the tunnel support and surrounding mass with the initial stress state σ_{ij}^0 in Eq. (1) prior to the formation of the working. All the changes in the rock mass SSS occur on constructing the lining. The problem is solved in terms of the additional displacements. In the lining, the initial stress is zero. Rigid adhesion of the rock mass and the lining ensures continuity of the surface force vector at contact; the stresses in the rock mass after driving the tunnel are $\sigma_{ij} = \sigma_{ij}^0 + \Delta\sigma_{ij}^0$, in the lining, $\Delta\sigma_{ij}^0$ is the additional stresses calculated from the additional displacements.

In the one-dimensional case (an initial hydrostatic stress state in the plane perpendicular to the tunnel and an axially symmetric circular lining), an analytical solution is obtained for the two formulations and test calculations are conducted.

In Fig. 2*b* (on the right), curve *1* is the stress distribution at the inner tunnel contour for the formulation in terms of the additional stresses. This formulation more adequately reflects the rock mass behavior and permits the estimation of the state of the lining with the shield method of creating a monolithic concrete tunnel.

Some problems may arise in analyzing the lining contact with the soil massif. The tangential surface forces at contact τ_n do not exceed $C + \sigma_n \mu$ on account of shear at the contact, where σ_n is the normal component of the surface force vector at contact; C is the adhesion; $\mu = \operatorname{tg}\varphi$ is the friction coefficient. In the limiting particular case where $C = 0$ and $\mu = 0$, the tangential component of the surface force vector at contact τ_n vanishes. The change in state of the lining is found by modeling.

We illustrate the analysis of the contact boundary interaction by an approach analogous to the boundary condition matching adopted in the boundary element method [6] for the example of rock mass consisting of two blocks. After discretization of the region into triangular elements, the grid nodes are numbered as follows. At each node on the contact boundary, a second node with the same coordinates is introduced. The number of elements is unchanged. As a result, node m at the contact belongs to the elements of the first block and node $m + 1$ belongs to the elements of the second block. To determine the displacements in the rock mass, matched conditions at the contact boundaries must be used. In the case of opening of the contact, the condition when the surface force vector is zero in this region of the contact is sufficient. Equality of the displacement vector at the double nodes ensures elastic behavior of the blocks of massif at contact. In the case of shear at the contact, the following two conditions are required: the equality of normal to the contact of the displacement vector component; and the tangential and normal components of the surface force vector are linearly related, in accordance with the Coulomb criterion.

At the contact of the lining with the soil mass, there are 67 nodes. After renumbering them, the number is doubled; contact node m belongs to the elements of the rock mass and node $m + 1$ to the elements of the lining (Fig. 3*a*). The two pairs of equations from the complete system of linear algebraic equations for the nodal displacements corresponding to nodes m and $m + 1$ take the form

$$b_1 u_m + b_2 \upsilon_m + \Sigma_u^m + X_m^0 = X_m, \quad b_2 u_m + b_3 \upsilon_m + \Sigma_\upsilon^m + Y_m^0 + P_m = Y_m$$

$$c_1 u_{m+1} + c_2 \upsilon_{m+1} + \Sigma_u^{m+1} = X_{m+1}, \quad c_2 u_{m+1} + c_3 \upsilon_{m+1} + \Sigma_\upsilon^{m+1} + P_{m+1} = Y_{m+1}, \tag{2}$$

where Σ_i^j is the sums of the form

$$\sum\nolimits_u^m = \sum_{k=1}^{N_m} a_{11}^m(i_k) u(i_k) + \sum_{k=1}^{N_m} a_{12}^m(i_k) \upsilon(i_k),$$

$$\sum\nolimits_\upsilon^m = \sum_{k=1}^{N_m} a_{21}^m(i_k) u(i_k) + \sum_{k=1}^{N_m} a_{22}^m(i_k) \upsilon(i_k),$$

$$\sum_u^{m+1} = \sum_{l=1}^{N_{m+1}} a_{11}^{m+1}(j_l)u(j_l) + \sum_{l=1}^{N_{m+1}} a_{12}^{m+1}(j_l)\upsilon(j_l),$$

$$\sum_\upsilon^{m+1} = \sum_{l=1}^{N_{m+1}} a_{21}^{m+1}(j_l)u(j_l) + \sum_{l=1}^{N_{m+1}} a_{22}^{m+1}(j_l)\upsilon(j_l).$$

The node m has N_m adjacent nodes numbered $i_1, i_2, \ldots i_{N_m}$; $u(i_k)$, $\upsilon(i_k)$ are the horizontal and vertical components of the displacement at node i_k. Correspondingly, node $m+1$ has N_{m+1} adjacent nodes numbered $j_1, j_2, \ldots j_{N_{m+1}}$, and $u(j_l)$, $\upsilon(j_l)$ are the horizontal and vertical components of the displacement at node j_l. Here and in what follows, the displacements are understood to be their additional values. The four Eqs. (2) from the complete system of linear algebraic equations determine how the displacements (u_m, υ_m) and $(u_{m+1}, \upsilon_{m+1})$ at the nodes m and $m+1$ are related to the displacements of the adjacent nodes. Note that

$$\begin{vmatrix} b_1 & b_2 \\ b_2 & b_3 \end{vmatrix} \quad \text{and} \quad \begin{vmatrix} c_1 & c_2 \\ c_2 & c_3 \end{vmatrix}$$

are symmetric 2×2 submatrices of the coefficients of the total rigidity matrix of the system located on its principal diagonal; their elements are, respectively, at the intersection of the rows and columns numbered $2m-1$, $2m$ and $2(m+1)-1$, $2(m+1)$ of the rigidity matrix.

Likewise

$$\begin{vmatrix} a_{11}^m(i_k) & a_{12}^m(i_k) \\ a_{21}^m(i_k) & a_{22}^m(i_k) \end{vmatrix} \quad \text{and} \quad \begin{vmatrix} a_{11}^{m+1}(j_l) & a_{12}^{m+1}(j_l) \\ a_{21}^{m+1}(j_l) & a_{22}^{m+1}(j_l) \end{vmatrix}$$

are 2×2 submatrices of the coefficients of the total rigidity matrix of the system; their elements are, respectively, at the intersection of the rows numbered $2m-1$, $2m$ and the columns numbered $2i_k-1$, $2i_k$ and also the rows numbered $2(m+1)-1$, $2(m+1)$ and the columns $2j_l-1$, $2j_l$. Also

$$\begin{vmatrix} X_m^0 \\ Y_m^0 \end{vmatrix}, \quad \begin{vmatrix} 0 \\ P_m \end{vmatrix}, \quad \begin{vmatrix} 0 \\ P_{m+1} \end{vmatrix}$$

are the contribution of the initial stresses and vertical gravitational forces of the elements of the rock mass containing node m and the contribution of the gravitational forces of the elements containing node $m+1$ to the nodal force, while

$$\begin{vmatrix} X_m \\ Y_m \end{vmatrix} \quad \text{and} \quad \begin{vmatrix} X_{m+1} \\ Y_{m+1} \end{vmatrix}$$

are surface force vectors localized at the nodes m and $m+1$, equal in the given plane case to the product of the corresponding surface force vectors at contact and the contact length $(L_1 + L_2)/2$ (Fig. 3*b*).

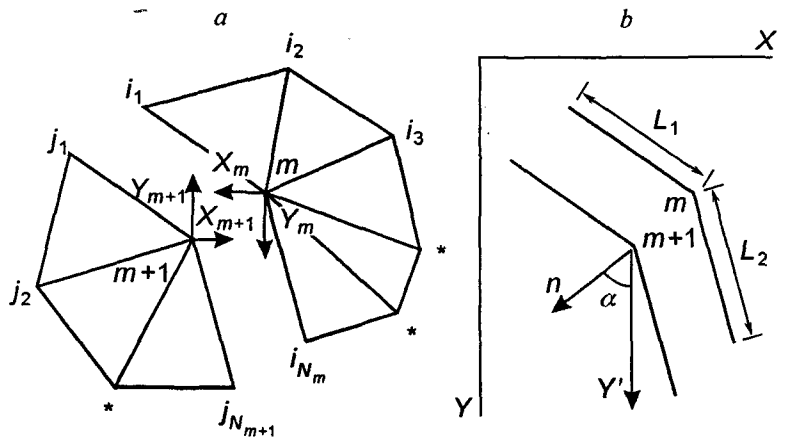

Fig. 3. Double nodes at the contact of soil massif with tunnel lining.

Thus, the four Eqs. (2) from the complete system of linear algebraic equations determine how the displacements (u_m, υ_m) and $(u_{m+1}, \upsilon_{m+1})$ at nodes m and $m+1$ are related to the displacements of the adjacent nodes. The case of contact opening corresponds to four Eqs. (2) with a zero right side (the surface force vector is zero), which is sufficient for determining the displacements of the double nodes. In the rest cases, due to equilibrium at the contact, the following conditions are required: $X_m + X_{m+1} = 0$ and $Y_m + Y_{m+1} = 0$. As a result, Eqs. (2) reduce to two relations

$$b_1 u_m + b_2 \upsilon_m + c_1 u_{m+1} + c_2 \upsilon_{m+1} + \Sigma_u^m + \Sigma_u^{m+1} + X_m^0 = 0,$$
$$b_2 u_m + b_3 \upsilon_m + c_2 u_{m+1} + c_3 \upsilon_{m+1} + \Sigma_\upsilon^m + \Sigma_\upsilon^{m+1} + Y_m^0 + P_m + P_{m+1} = 0. \quad (3)$$

To determine the displacements at the double nodes, two additional conditions characterizing the behavior of the contact must be employed. In the case of shear of the contact sides, these conditions correspond to equal displacement vector components normal to the contact at the double nodes

$$u_m \cos\alpha + \upsilon_m \sin\alpha = u_{m+1} \cos\alpha + \upsilon_{m+1} \sin\alpha \quad (4)$$

and zero tangential component of the surface force vector at contact

$$-X_m \sin\alpha + Y_m \cos\alpha = 0,$$

which leads to the second additional equation for the displacements at the double nodes of the contact

$$-(b_1 u_m + b_2 \upsilon_m)\sin\alpha + (b_2 u_m + b_3 \upsilon_m)\cos\alpha - (\Sigma_u^m + X_m^0)\sin\alpha + (\Sigma_\upsilon^m + Y_m^0 + P_m)\cos\alpha = 0, \quad (5)$$

where α is the angle between the normal to the contact and the vertical axis (Fig. 3*b*). Rigid adhesion of the sides of the contact ($u_m = u_{m+1}$ and $\upsilon_m = \upsilon_{m+1}$ ensures elastic behavior of the rock mass when there is no shear along the contact and no opening of its sides.

In the first stage, the problem is solved with rigid adhesion of the double nodes at the rock mass–lining contact; this is equivalent to the elastic solution obtained earlier. Then, at all the contact nodes, except for two on the symmetry axis (for which $u_m = u_{m+1} = 0$ and $\upsilon_m = \upsilon_{m+1}$), shear conditions at the contact are specified: Eqs. (3)–(5). The stress distribution at the inner tunnel contour in this case is shown by curve *2* in Fig. 2*b* (on the right); the soil mass shear at contact is shown on the left (positive values correspond to counter-clockwise shear of the soil mass). Despite the considerable shear of the soil mass (2 cm), the formulation of the problem taking contact shear into account leads to no significant changes in stress state of the tunnel lining, even in the given limiting case with no tangential stresses at the contact. In reality, in the presence of adhesion and friction at the contact of soil mass with lining, the stresses at the inner tunnel contour is within the region indicated in Fig. 2*b* (on the right).

Note that these results differ significantly from those obtained in the direct formulation. There are no tensions in the lining, and the compressive stresses (1–4 MPa) are considerably less than the uniaxial compression strength of concrete.

2. MODELING ROCK MASS STATE IN THE PRESENCE OF FRACTURES

The approach to modeling the contact interaction of a block massif proposed in the preceding section is used to determine the deformation of rock mass with a geological disturbance. The presence of adhesion and friction at the contact in shear over the fracture surface, according to the condition $\tau_n = C + \sigma_n \mu$, leads to the following additional equation

$$\frac{L_1 + L_2}{2}\left|-X_m \sin\alpha + Y_m \cos\alpha\right| = C + (X_m \cos\alpha + Y_m \sin\alpha)\frac{L_1 + L_2}{2}\mu.$$

The adhesion C for fractures with no roughness (of the order of a few MPa) may be neglected in modeling the fracture behavior at $H \sim 1$ km ($\gamma H \approx 30$ MPa). Modeling with friction coefficient $\mu = 0.5$ and adhesion $C = 0$ permits estimation of the maximum change in rock mass stress state in the presence of fractures in comparison with the elastic solution for most rocks [7]. The typical conditions of the deep Talnakh mines are assumed in modeling.

The Case Where the Face Approaches a Vertical Geological Disturbance

At a depth $H = 1$ km, there is a mined-out space of width around 250 m and height 25 m. The initial stress state of the rock mass is specified so that the vertical and horizontal components of the initial stress field are equal at a depth H:

$$\sigma_x^0 = \frac{1-2\nu_m}{1-\nu_m}\gamma_m H + \frac{\nu_m}{1-\nu_m}\gamma_m y, \quad \sigma_y^0 = \gamma_m y, \quad \tau_{xy}^0 = 0,$$

where $\gamma_m = 0.027$ MPa/m is the specific weight, $\nu_m = 0.25$ is its Poisson's ratio of the massif, and y is the distance from the surface. The strain modulus of the rock mass $E_m = 40$ GPa. The size of the total region is 4×4 km. The boundary conditions for the formulation in terms of the additional stresses are analogous to those already given. The number of grid nodes and elements is 2205 and 4254, respectively; the minimum size of an element close to the mined-out space is around 3 m. The behavior of a vertical fracture in the rock mass on approaching the breakage face is investigated. The distributions of the vertical stress tensor component on the horizontal line $y = H = 1$ km (support pressure curve) with decrease in the width of the pillar l_p between the fracture and the face ($l_p = 9, 6, 3$, and 0 m) are shown in Fig. 4*a*. In the first stage, for each case, rigid adhesion of the sides of the fracture is considered; this is analogous to elastic behavior of the rock mass as a whole. If the tangential component τ_n of the surface force vector at the fracture surface exceeded the product of the normal component σ_n of the surface force vector and the friction coefficient $\mu = 0.5$, shear along the fracture is specified at some nodes with the maximum tangential component of the surface force vector. Five iterations are required to determine the SSS of rock mass with a fracture at the maximum contact shears ($l_p = 0$; the lowest curve in Fig. 4). In Fig. 4*b*, the shears of the fracture sides for each calculation variant are shown. Analysis of the results leads to the following conclusions. A vertical geological disturbance begins to affect the rock mass behavior when the approaching extraction front reaches a distance of around 9 m to the fracture. Shears along the fracture begin at a height of around 40 m above the horizontal line of the roof of the mined-out space. An increase in rock pressure in the pillar beyond the fracture relative to the rock mass is recorded. The vertical geological disturbance acts as a screen preventing the propagation of the supporting pressure to the rock mass. The lower curve in Fig. 4 illustrates the asymmetry in the support pressure curve when the breakage face is at the fracture. The maximum vertical stresses at the right mining operation front exceed the corresponding values at the left front by about 20 MPa. Note the slight difference ($\gamma_m H = 27$ MPa) introduced by such a seemingly significant factor as an extended vertical geological disturbance at one of the fronts of deposit. The basic risk when the extraction front approaches a vertical fracture is the possible dynamic rock pressure manifestations when mining pillar with a width less than a quarter of the ledge thickness (the strength of the ores and rocks in the Talnakh mine in uniaxial compression is of the order of 100 MPa) [8].

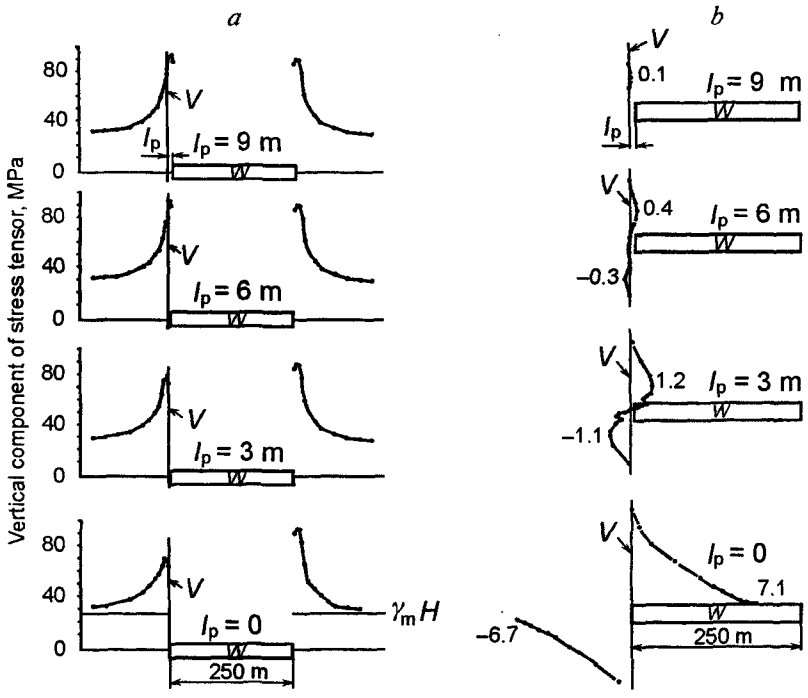

Fig. 4. *a*) Support pressure in successive approaching operation front to a vertical geological disturbance; the distance from the fracture to the boundary of mined-out space decreases from 9 m (upper graph) to 0 m (lower graph); *b*) shear of the sides of a vertical geological disturbance (cm) as the mined-out space approaches; *W* denotes the mined-out space, and *V* denotes the vertical fracture.

Horizontal Geological Disturbance above Mined-Out Space

The influence of a horizontal fracture at a height of 25 m above the roof of a mined-out space (height 25 m and width 250 m) formed as a result of mining a reserve of ore ledge at depth of 1 km is now considered by modeling. The size of the complete region, the boundary conditions, the initial stress state, the deformation properties of the rock mass, and the strength properties of the geological disturbance are analogous to those in the preceding case. On account of the symmetry, half of the total solution region is considered. The number of grid nodes and elements is 1061 and 1926, respectively; the minimum size of an element in the vicinity of the mined-out space is around 6 m. In the first stage, the problem is solved for rigid adhesion of the sides of the fracture, modeling the elastic behavior of the rock mass as a whole. The solid curves in Fig. 5 show the convergence of the roof and floor of the mined-out space and the support pressure curve. Then, successively from iteration to iteration, the condition of contact opening is specified in the section of the fracture where the normal surface forces are tensile, and the shear condition is specified in the section where τ_n exceeds $\sigma_n \mu$. Altogether, six iterations are required. The dashed curve in Fig. 5*a* shows the convergence of the roof and floor of the mined-out space. The zones of opening, shear, and rigid adhesion of the fracture sides are shown in Fig. 5*b*, along with the magnitudes of the fracture opening and shear. In Fig. 5*c*, the distributions of the tangential and normal components of the surface force vector at contact are shown. Note the slight overall influence of the fracture on the rock mass SSS. The support pressure curve is practically unchanged (points in Fig. 5*a*), and the convergence of the roof and floor of the mined-out space increases by approximately the magnitude of fracture opening (less than 7 cm). The basic risk in mining operation development with a horizontal geological disturbance above the mined-out space is stability loss of the ascending workings and boreholes in the fracture side shear zone. A maximum shear of around 5 cm may disrupt the support of the ascending workings and will require additional expenditures to restore them.

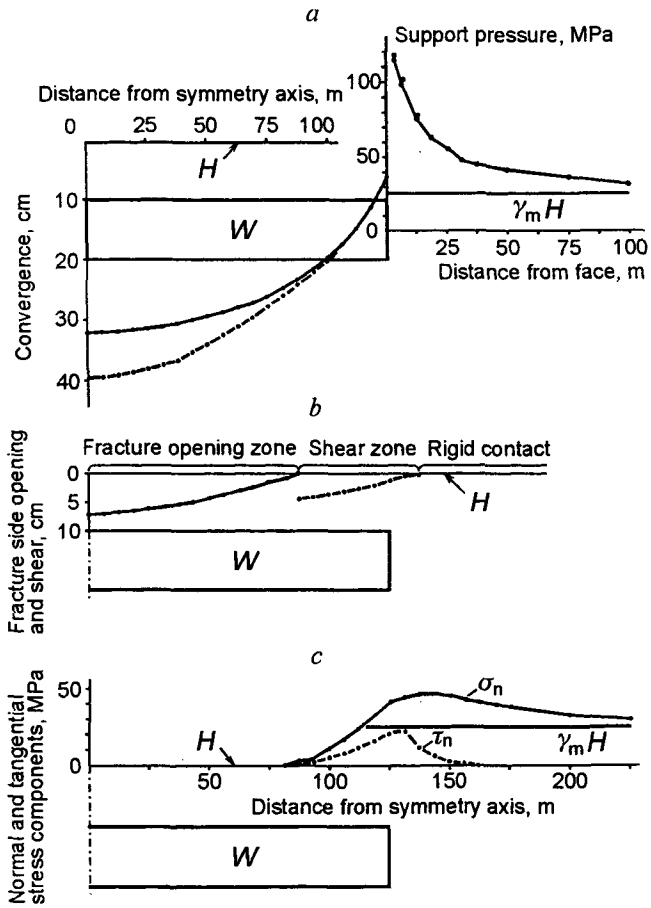

Fig. 5. Convergence of roof and floor of the mined-out space and support pressure without fracture (solid curves) and with (dash-dot curves) a horizontal geological disturbance (*a*), opening and slip of fracture sides (*b*), and distribution of the normal and tangential stress components at the fracture surface (*c*); *W* denotes the mined-out space, and *H* denotes the horizontal fracture.

CONCLUSIONS

A grid of triangular elements may be constructed by means of programs implementing the improved algorithm for automatic discretization of the solution region in [9], which permits an arbitrary configuration of the regions where the grid is denser. The system of linear algebraic equations for determining nodal displacements is solved iteratively by successive upper relaxation, with an accelerating factor of 1.8–1.9. The feature of the calculation scheme is that the elements of the rigidity matrix are calculated as required in the iterative method of solution of set of equations. This permits significant reduction in the demands on the short-term computer memory.

The results obtained permit the following conclusions.

1. In solving geomechanical problems, the "direct" formulation and the formulation in terms of the additional stresses must be distinguished. For the stowing materials used in the deep Talnakh mines, the "direct" formulation may be used to estimate the state of the artificial massifs. However, when the depth is small (in comparison with the width of the working) or the strain moduli of the stowing and the rock mass are of the same order, approaches more adequately reflecting the technology of formation of mined-out spaces filled with stowing are required. The formulation in terms of additional stresses more accurately reflects the actual rock mass behavior, with only slight expenditures to amend the programs for the "direct" formulation.

2. A method for modeling continuity disturbances in rock mass has been proposed as an alternative to the contact-element widely used in FEM [10]. The contact is the internal boundary of a region with double nodes belonging to the contacting subregions, for which, as usual, independent systems of linear algebraic equations in terms of the nodal displacements are determined. The complete system of equations is formulated by the introduction of additional matched boundary conditions at the contact corresponding to rigid adhesion, opening of the fracture, or shear of its sides. This approximate approach is justified when there are no reliable data on the deformational properties of the geological disturbances.

REFERENCES

1. I. V. Rodin, "Released load and rock pressure," in: *Rock Pressure Investigations* [in Russian], Gosgortekhizdat, Moscow (1960).
2. D. H. Trollop, H. Bock, B. S. Best, et al., *Introduction to the Mechanics of Jointed Rock* [Russian translation], Mir, Moscow (1983).
3. O. Zenkevich, *Finite-Element Method in Engineering* [Russian translation], Mir, Moscow (1975).
4. S. V. Kuznetsov, V. N. Odintsov, M. E. Slonim, and V. A. Trofimov, *Methodology of Rock Pressure Calculation* [in Russian], Nauka, Moscow (1981).
5. I. L. Boltengagen, S. N. Popov, and V. M. Seryakov, "Character of Elastic deformation of tunnel lining in rock mass," in: *Mathematical Methods and Computer Techniques in Mining* [in Russian], IGD SO AN SSSR, Novosibirsk (1987).
6. S. Crouch and A. Starfield, *Boundary-Element Methods in Solid-State Mechanics* [Russian translation], Mir, Moscow (1987).
7. Yu. M. Kartashov, B. V. Matveyev, G. V. Mikheyev, and A. B. Fadeyev, *Strength and Deformability of Rocks* [in Russian], Nedra, Moscow (1979).
8. Ye. I. Ilnitskaya, R. I. Teder, Ye. S. Vatolin, and M. F. Kuntysh, *Rock Properties and Methods of Their Determination* [in Russian], Nedra, Moscow (1969).
9. I. L. Boltengagen, M. V. Kurlenya, and S. N. Popov, "Automated construction of a grid of triangular elements in two-dimensional multiply connected regions," in: *Analytical and Numerical Researches in Rock Mechanics* [in Russian], IGD SO AN SSSR, Novosibirsk (1986).
10. R. E. Goodman, R. L. Taylor, and T. L. Brekke, "A model for the mechanics of jointed rock," *J. Soil Mech. Found. Div.*, No. 3 (1968).